

M4Human: A Large-Scale Multimodal mmWave Radar Benchmark for Human Mesh Reconstruction

Junqiao Fan¹ Yunjiao Zhou¹ Yizhuo Yang¹ Xinyuan Cui^{2,5} Jiarui Zhang¹

Lihua Xie¹ Jianfei Yang¹ Chris Xiaoxuan Lu³ Fangqiang Ding^{4,5 *}

¹Nanyang Technological University ²University of Pennsylvania ³University College London
⁴Massachusetts Institute of Technology ⁵University of Edinburgh

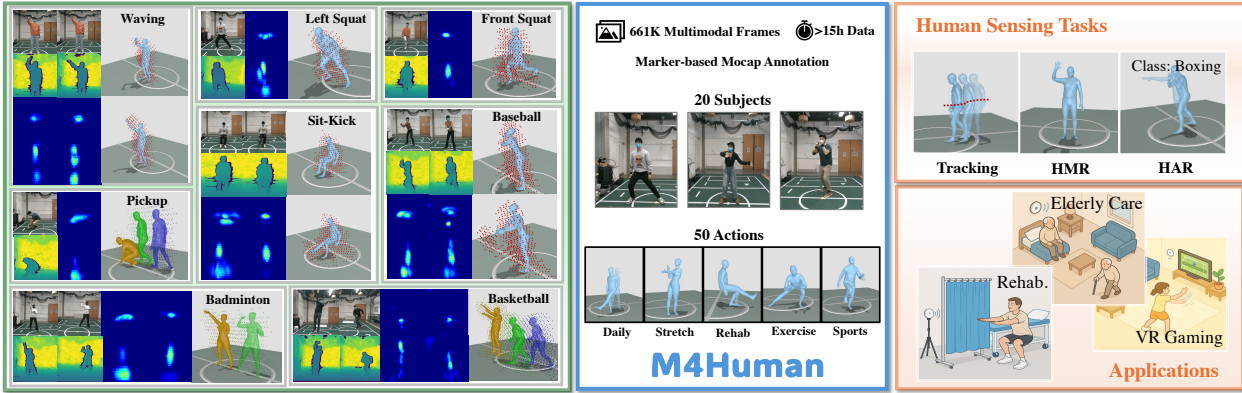


Figure 1. M4Human is the largest multimodal dataset for high-fidelity RF-based mmWave radar human sensing (e.g., HMR). M4Human extends beyond simple in-place actions to complex free-space motions (e.g., rehab, exercise and sports), which is supported by high-quality MoCap annotations. Its diversity enables a wide spectrum of human sensing tasks and privacy-preserving applications.

Abstract

Human mesh reconstruction (HMR) provides direct insights into body-environment interaction, which enables various immersive applications. While existing large-scale HMR datasets rely heavily on line-of-sight RGB input, vision-based sensing is limited by occlusion, lighting variation, and privacy concerns. To overcome these limitations, recent efforts have explored radio-frequency (RF) mmWave radar for privacy-preserving indoor human sensing. However, current radar datasets are constrained by sparse skeleton labels, limited scale, and simple in-place actions. To advance the HMR research community, we introduce M4Human, the current largest-scale (661K-frame) (9× prior largest) multimodal benchmark, featuring high-resolution mmWave radar, RGB, and depth data. M4Human provides both raw radar tensors (RT) and processed radar point clouds (RPC) to enable research across different levels of RF signal granularity. M4Human includes high-quality motion capture (MoCap) annotations with 3D meshes and global trajectories, and spans 20 subjects and 50 diverse actions, including in-place,

sit-in-place, and free-space sports or rehabilitation movements. We establish benchmarks on both RT and RPC modalities, as well as multimodal fusion with RGB-D modalities. Extensive results highlight the significance of M4Human for radar-based human modeling while revealing persistent challenges under fast, unconstrained motion. The dataset and code will be released after the paper publication.¹

1. Introduction

Perceiving 3D human motion is essential for human-centric Physical AI systems to understand users' behavior and respond to their needs. A key enabler is markerless 3D human pose and shape regression, a core human sensing task that supports many applications such as human-robot interaction, rehabilitation, healthcare monitoring, surveillance, and VR/AR [6, 38]. Classic human pose estimation (HPE) represents the human body as a graph of keypoints and infers their 3D locations [51]. Moving beyond sparse landmarks, human mesh reconstruction (HMR) estimates both pose and shape of the human body as a dense surface mesh that can be used to model human-environment contact, enabling advanced applications such as VR fitness gaming,

^{*}F. Ding is the corresponding author.

¹Project page

virtual try-on, avatar creation, and computer-assisted coaching [29, 39]. However, current HMR systems are predominantly built on Line-of-Sight (LoS) camera (e.g., RGB and depth) and trained on large-scale video datasets (e.g., Human3.6M [22], 3DPW [40]). This raise two practical issues: (i) visual data exposes personal appearance, often inaccessible for privacy-sensitive scenarios, such as children and elderly care, and public sharing is frequently restricted [31]; (ii) LoS cameras are usually vulnerable to adverse illumination like low-lighting and strong sunlight, and susceptible to occlusion, such as thick clothing or smoke [7, 11].

There is a growing interest in millimeter-wave (mmWave) radar-based human sensing, positioning it as a complement, or even an alternative to vision-based systems [46]. As a radio-frequency (RF) sensor, mmWave radar actively emits radio waves to sense human targets and analyzes the returned echoes to recover spatial information (range and angle) [34]. This sensing principle enables deployment in complex real-world conditions, with robustness to variable illumination and occlusion, while preserving user privacy and facilitating data distribution. Moreover, mmWave radar operates in a higher-frequency band (e.g., 77GHz), offering higher spatial resolution than other RF sensors (e.g., Wi-Fi), making it well-suited for HMR that demands fine-grained data.

Despite these advantages, existing large-scale HMR datasets/benchmarks remain largely RGB image-centric, with mmWave-based approaches rarely explored. As summarized in Tab. 1, most existing mmWave radar-based human sensing datasets [3, 5, 20, 33, 44, 48] are oriented for coarse-grained HPE and provide only sparse skeleton annotations. These labels are typically derived from RGB(D) cameras via existing pose estimators or multi-view optimization and thus inevitably noisy, introducing ground-truth (GT) bias that hinders high-fidelity sensing. Two RF-based HMR datasets have recently been released [7, 43], but they remain limited in scale and focus primarily on simple, in-place daily activities, constraining their application to dynamic and diverse scenarios. In terms of the modality, most datasets rely on low-resolution Texas Instruments (TI) radars that output only very sparse radar point clouds (RPC) [17], discarding much valuable signal information. While recent efforts [20, 33] have begun to explore raw radar tensors (RT) to preserve more contextual information, they remain centered on coarse-level HPE and do not support fine-grained HMR.

To bridge this gap, we introduce M4Human, the largest-scale multimodal dataset that supports high-fidelity RF-based HMR. It comprises 999 sequences and 661K (>15 h) synchronized samples across RGB and depth images plus multi-level radar data—raw tensors (RT) and point clouds (RPC)—captured by a high-resolution Vayyar mmWave radar tailored to human sensing. M4Human includes high-quality marker-based motion capture (MoCap) annotations to provide 3D HMR GT, along with an abundant set of metic-

ulously designed daily, rehabilitation, and sports activities. To the best of our knowledge, M4Human is the first and largest benchmark (about $9\times$ larger than the prior largest mmBody [7]) to enable mmWave tensor-based HMR across diverse, dynamic, and unconstrained indoor scenarios. Its key features and contributions are summarized as follows:

- **Complementary Sensing Modalities.** M4Human contributes to multimodal human sensing by combining complementary sensing modalities, including line-of-sight (LoS) cameras and radio-frequency (RF) mmWave radar. It provides four synchronized modalities: RGB frames, depth frames, raw radar tensors (RT), and radar point clouds (RPC). The inclusion of both raw and processed radar data supports research at different levels of RF signal processing and understanding.
- **High-Fidelity Motion Annotations.** The dataset includes marker-based motion capture (MoCap) annotations to support high-quality GT annotation, including 3D human mesh, human dense pose, 2D/3D skeleton keypoints, full-body position tracking under dynamic free-space sport activities, and abundant action categories.
- **Diverse Action Sets.** M4Human includes 50 categories of human actions, spanning in-place daily activities, clinically guided rehabilitation exercises, and non-in-place sports motions. This diversity supports applications in smart home, healthcare research (e.g., evaluation and rehabilitation of neurological or physical impairments), and human-computer interaction (e.g., virtual fitness gaming).
- **Wide Human Sensing Tasks.** The high-quality motion annotations in M4Human enable novel tasks such as simultaneous human tracking and mesh reconstruction under free-space and complex sports motions. The rich data modalities further support multi-modal fusion and cross-modal supervision for RF-based human sensing. M4Human also supports critical research problems, including HMR using different radar modalities, and generalization across unseen subjects and action categories.
- **Extensive Benchmarks.** To support and evaluate radar-based HMR, M4Human benchmarks state-of-the-art (SOTA) methods on both raw radar tensors (RT) and radar point clouds (RPC). We further compare with RGB-D modalities and evaluate the fusion of radar and visual RGB-D data for enhanced mesh reconstruction. We analyze model performance under varying dataset scales, highlighting the importance of large-scale datasets. Finally, we validate the effectiveness of radar-based HMR in supporting downstream human activity recognition.

2. Related Works

mmWave-based Human Sensing. RGB cameras are ubiquitous for human sensing tasks (e.g., HMR [13, 25]), but raise privacy concerns in sensitive settings and degrade under occlusion and poor lighting [8]. As reported in [7], camera-

Table 1. Comparison of M4Human with prior datasets († denotes non-public data). Overall, M4Human is the largest RF-based dataset with multi-granularity motion annotations across diverse sensing tasks. It provides both raw radar tensors (RT) and filtered radar point clouds (RPC) for high-fidelity HMR, and extends beyond simple in-place activities to complex, non-in-place rehabilitation and sports. Human body annotations are obtained with a high-precision marker-based MoCap system rather than RGB(D) images (entries marked with *)

Task	Dataset		Modalities			Annotations			Statistics				Actions			
	Name	RF-BW(GHz)	RGB	Depth	mmWave	Actions	Global-Traj.	Skeleton	Mesh	# Act.	# Sub.	# Seq.	# Frame	Daily	Rehab.	Sports
RGB-based HMR	MPI-INF-3DHP [30]	-	✓			✓	✓	3D	✓	8	8	16	1.3M	✓		
	Human 3.6M [22]	-	✓			✓	✓	3D	✓	17	11	210	3.6M	✓		
	3DPW [40]	-	✓			✓	✓	3D	✓	-	7	60	>51K	✓		
RF-based HPE	mRI [5]	77-81	✓	✓	RPC	✓		3D*		12	20	300	160K	✓	✓	
	MARS [3]	77-81	✓		RPC	✓		3D*		10	4	80	40K	✓		
	RF-Pose3D† [48]	77-81			RT	✓		3D*		5	>5	-	-	✓		
	HrPR [26]	77-81			RT			2D*		3	6	235	141K	✓		
	mm-Fi [44]	60-64	✓	✓	RPC	✓		3D*		27	40	1080	320K	✓	✓	
	RT-Pose [20]	77-81	✓	✓	RT		✓*	3D*		6	-	240	72K	✓		
RF-based HMR	MMVR [33]	77-81	✓		RT			2D*		-	25	395	345K	✓		
	mmMesh† [43]	77-81			RPC			3D	✓	8	20	34	3K	✓		
	mmBody [7]	76-81	✓	✓	RPC	✓		3D	✓	<30	20	48	<70K	✓		
	M4Human (ours)	62-69	✓	✓	RT & RPC	✓	✓	3D	✓	50	20	999	661K	✓	✓	✓

based methods suffer remarkable error increases: depth (rain 56.4%, smoke 336%), RGB (dark 42.8%, smoke 16.2%) on HMR. Commercial mmWave radar has therefore emerged as a privacy-preserving and robust complement for indoor human sensing. Early radar-based works used low-resolution RPCs to tackle coarse-level motion tracking [9, 19, 47, 50], where human motion was reduced to a single-point trajectory and tracked using clustering and RNNs under simple walking scenarios. Subsequent studies targeted human action recognition for daily actions and HCI gestures [2, 27, 28, 37]. More recently, whole-body keypoint estimation from sparse RPCs has been explored via datasets and methods such as mRI, mm-Fi, and others [3–5, 10, 15, 35, 44]. To alleviate the information loss during radar point cloud generation, RETR [45], RT-Pose [20] and more [26, 33, 42] operate directly on raw radar tensors for human pose estimation. A few recent works, such as mmBody [7] and mmMesh [43], investigate mesh reconstruction from RPCs, but they remain limited to daily actions and in data scale, which limits their application scope and generalizability. To date, no works have explored RT-based HMR.

mmWave-based Human Pose Datasets. The success of RGB-based HMR methods has been driven by large-scale image-based datasets (e.g., MPI-INF-3DHP [30], Human3.6M [22], 3DPW [40]), which provide high-quality 3D annotations from marker-based or markerless multi-view MoCap systems. In contrast, early mmWave HPE datasets [3, 48] focus on simple in-place daily activities and provide only sparse RPC from low-resolution (LR) radars (e.g., 4 Tx/Rx channels, 4 GHz bandwidth; see Table 1). mRI [5] and mm-Fi [44] expand to in-place rehabilitation movements but still rely on synchronized RGB to annotate 3D skeletons, which is inevitably noisy and hard to support high-fidelity human sensing. More recent datasets [26, 42], such as MMVR [33], RT-Pose [20], explore raw radar tensors (RT) for coarse-grained HPE, often using cascaded LR

radar chips or multi-view setups to boost spatial resolution at the cost of harder synchronization and calibration. For HMR, mmMesh [43] first reconstructs MoCap-annotated meshes from LR RPC, but its dataset is not publicly available. mmBody [7], employs a high-resolution automotive radar for indoor perception but lacks access to more informative RT data. Moreover, its RPC contains substantial background returns, leaving only a small fraction from the human foreground (c.f. Fig. 2(a)). In addition, existing radar datasets remain limited in scale and largely restricted to simple, in-place actions, which constrains their utility for broader and more dynamic human activities (c.f. Fig. 2(b)).

3. Datasets

Overview. At the core of our contribution is M4Human, a large-scale multimodal dataset designed for fine-grained human mesh reconstruction (HMR). As illustrated in Fig. 3, we build a unified sensing platform that integrates a high-resolution mmWave radar, an RGB-D camera, and a Vicon MoCap system. During capture, subjects are instructed to perform a diverse set of actions while the RGB-D camera and radar record synchronized multimodal data, and the Vicon system captures precise 3D marker positions for accurate mesh annotations. Our dataset is characterized by (i) *diversity*: 661K frames across 999 sequences, involving 20 subjects and 50 meticulously designed action classes; (ii) *multimodality*: synchronized RGB, depth, radar point cloud (RPC), and raw radar tensor (RT) with precise cross-modal calibration; (iii) *high-quality annotation*: dense and time-aligned 3D meshes derived from marker-based Vicon capture with human-in-the-loop verification.

3.1. System Setup

We use an Intel RealSense D435 stereo depth camera [21] that integrates an IR projector, an RGB camera, and a stereo IR pair to acquire synchronized RGB-D image frames. Raw

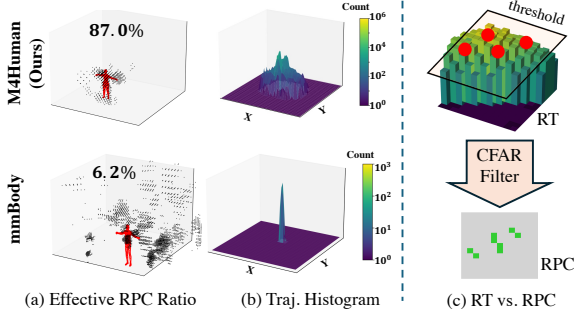


Figure 2. Comparison between M4Human and mmBody [7]: (a) M4Human achieves a much higher effective RPC ratio around human subjects. (b) M4Human is much larger in scale and involves more diverse global trajectories than simple in-place daily activities of mmBody. (c) M4Human provides additional raw RT modality that contain more unfiltered information than RPC.

resolution is up to 1280×720 ; for storage efficiency and faster I/O, we downsample to 640×480 . mmWave data are captured using the commercial Vayyar vTrigB imaging mmWave radar [1]. The device integrates a proprietary human-sensing mmWave Software on Chip (SoC) and outputs both raw radar tensors (RT) and processed radar point clouds (RPC). With 7 GHz bandwidth and a large 20 Tx/Rx antenna array, it provides markedly better range and angular resolution than common 3-4 Tx/Rx TI radars [34]. The mmWave radar and RGB-D camera are mounted on a 3D-printed bracket fixed to a tripod (c.f. Fig. 3 (a)), connected to a unified recording PC. Subjects are recorded at distances of 0.5–6 m from the platform, within a motion area of approximately $6 \times 5.5 \text{m}^2$, with multiple facing orientations for data diversity. A Vicon MoCap system is installed overhead, providing high-precision position measurements of 3D markers attached to anatomical keypoints during action execution.

3.2. Human-centric and Multi-level Radar Data

The Vayyar radar used in M4Human is tailored to fine-grained human sensing. To show its superior sensing ability, we define an *effective RPC ratio* metric as the fraction of points near humans relative to all points per frame (c.f. Fig. 2(a)). M4Human attains a substantially higher effective RPC ratio than mmBody [7], which employed automotive radars designed for broad scene sensing rather than human targets, yielding much more background targets. With more human-concentrated returns, M4Human supports simultaneous global tracking and high-fidelity mesh reconstruction for diverse, non-in-place dynamic activities in open spaces. Furthermore, M4Human provides two complementary radar modalities: raw radar tensor (RT) and radar point cloud (RPC). RT is a 3D intensity volume obtained via FFT-based processing of time-domain signals across range, azimuth, and elevation axes, then mapped into Cartesian coordinates (X-Y-Z). RPC is derived from RT using CFAR [17], which

retains only salient reflections above adaptive thresholds. As illustrated in Fig. 2(c), CFAR removes sub-threshold structures and suppresses much of the spatial intensity context. Therefore, RT generally contains richer information than RPC. To support clearer interpretation and more comprehensive learning from mmWave signals, M4Human releases both RT and RPC modalities for public usage.

3.3. Calibration

For spatial calibration between the Vicon system and sensor platform, we affix six non-coplanar MoCap markers to a chair placed in the motion area (Fig. 3 (b)). We record their 3D positions in the Vicon frame \mathbf{X}_i^V ($i \in [1, \dots, 6]$) and manually annotate the corresponding 2D pixel locations \mathbf{x}_i in the RGB image. With chessboard-calibrated camera intrinsics $\mathbf{K} \in \mathbb{R}^{3 \times 3}$, we solve a Perspective-n-Point (PnP) problem [16] to estimate the camera extrinsics $(\mathbf{R}_{C \leftarrow V}, \mathbf{t}_{C \leftarrow V})$, such that $\mathbf{x}_i \sim \mathbf{K}(\mathbf{R}_{C \leftarrow V} \mathbf{X}_i^V + \mathbf{t}_{C \leftarrow V})$. We obtain the radar-camera extrinsic calibration $(\mathbf{R}_{C \leftarrow R}, \mathbf{t}_{C \leftarrow R})$ following a similar procedure but using radar-visible targets (e.g., corner reflectors) instead of MoCap markers. With both transformations, any 3D Vicon point \mathbf{P}^V can be first transformed into the camera frame as $\mathbf{P}^C = \mathbf{R}_{C \leftarrow V} \mathbf{P}^V + \mathbf{t}_{C \leftarrow V}$, and then to the radar frame via $\mathbf{P}^R = \mathbf{R}_{C \leftarrow R}^{-1}(\mathbf{P}^C - \mathbf{t}_{C \leftarrow R})$. This calibration process yields precise cross-modal alignment among the Vicon, RGB-D camera, and radar data.

3.4. Time Synchronization

In our setup, the Vicon system and the sensor board run on separate PCs. Radar and RGB-D streams are polled alternately at 12Hz by the same PC, yielding well-aligned sensor frames. To synchronize with Vicon, subjects are instructed to perform a *trigger* gesture when recording starts: after a T-pose, they rapidly swing their head to the right (c.f. Fig. 3 (c)). We detect the Vicon start frame as the first time the head-top marker’s displacement exceeds 10 cm, and we manually locate the corresponding RGB start frame and trim earlier radar/RGB-D frames accordingly. Because the Vicon stream has a higher frame rate (100Hz), each sensor frame is then temporally matched to its nearest Vicon frame.

3.5. Subjects and Actions

Subjects. M4Human dataset features a high diversity of human subjects, comprising 20 volunteers with varied heights (1.5–1.8m) and weights (45–90kg), balanced genders (12 male, 8 female), and heterogeneous ethnic backgrounds. This wide range of subject attributes ensures the dataset’s versatility and generalizability to a broad population. All participants have been informed that the data will be made publicly available for research purposes, and were instructed to wear caps and masks for de-identification.

Actions. M4Human meticulously curates 50 actions spanning three categories: (i) *daily activities* (e.g., waving, walk-

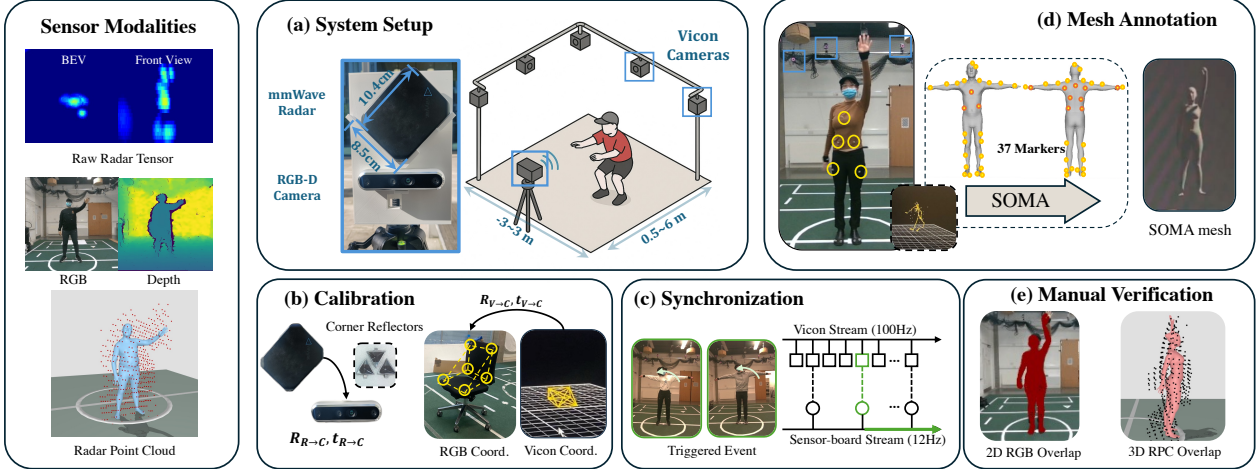


Figure 3. Overview of the system setup. M4Human designs a multimodal sensing platform with high-precision marker-based MoCap system. Appropriate calibration and synchronization workflow are designed for accurate alignment between modalities and annotations.

ing in a curve, sit-and-stand), targeting smart-home applications and human–computer interaction; (ii) *rehabilitation exercises* (e.g., upper limb extension, high knees) motivated by clinical practice to support routine training [49] and recovery assessment [24] in healthcare applications; and (iii) non-in-place *sports actions* (e.g., basketball, badminton) that require substantial whole-body coordination, supporting dynamic motion analysis and VR/AR applications.

During capture, each subject performs all 50 actions, with at least 550 frames captured per action at 12 Hz. This led to a total of 999 valid sequences, $\sim 661\text{K}$ valid synchronized multimodal frames, and ~ 15.3 hours of motion capture.

3.6. Body Mesh Annotation

We obtain high-precision human body mesh annotations via a three-stage pipeline. (i) *Marker-based capture*. We record human motion with a Vicon MoCap system that tracks the subject as a non-rigid body parameterized by 37 anatomically distributed markers (Fig. 3 (d)). This yields accurate 3D whole-body trajectories and stable root motion, providing higher-fidelity labels than the purely image-based annotation approaches common in prior RF datasets. (ii) *Human-in-the-loop cleanup*. The automatically labeled Vicon sequences are inspected frame by frame to correct typical MoCap errors (marker swaps, short-term occlusions, missing markers), so that the final marker trajectories are temporally consistent, stable, and avoid drifting. (iii) *Mesh reconstruction and validation*. Cleaned marker trajectories are fed to SOMA [18], a neural marker-to-body reconstructor, to estimate full-body pose, global trajectories, and SMPL-X-style meshes [32]. The reconstructed meshes and joints are then visualized together with the RGB-D and mmWave data to verify spatial-temporal alignment (Fig. 3 (e)).

4. Benchmark and Evaluation

Overview. M4Human enables a comprehensive benchmark across sensing modalities and tasks. We evaluate mmWave-based HMR with two radar representations, RPC and RT (Sec. 5.1); comparing radar- and image-based HMR to quantify each modality’s strengths and remaining gaps (Sec. 5.3); and exploring modality fusion to show how mmWave radar benefits multimodal HMR (Sec. 5.4). Since no prior works have used RTs for HMR, we propose a simple baseline supporting the RT modality (Sec. 4.2). We further demonstrate that the scale of M4Human improves the generalizability of radar-based HMR (Sec. 5.2), and that radar-predicted human meshes support downstream human action recognition (HAR) (Sec. 5.5).

4.1. Benchmark Setup

Protocol. We define three evaluation protocols aligned with action groups to assess performance under varying difficulty levels. Protocol 1 (P1) covers 30 *in-place* daily and rehabilitation activities. Protocol 2 (P2) focuses on five *sit-in-place* daily and rehabilitation exercises. Protocol 3 (P3) comprises all *non-in-place* daily/sports activities, which are more challenging due to larger displacements and rapid motion. We also report results on the full set (ALL).

Split. The dataset is divided into train/val/test with a ratio of 75:5:20, yielding $\sim 496\text{K}/34\text{K}/132\text{K}$ samples. We evaluate under three split settings: (S1) Random, all clips are randomly assigned to non-overlapping subsets, modeling seen-subject and seen-action cases; (S2) Cross-Subject, no subject in training appears in testing (two males and two females), modeling unseen-subject generalization; (S3) Cross-Action, a *group-stratified* split with disjoint action classes; the test set includes 20% of classes sampled from each action group (i.e., in-place, sit-in-place, non-in-place),

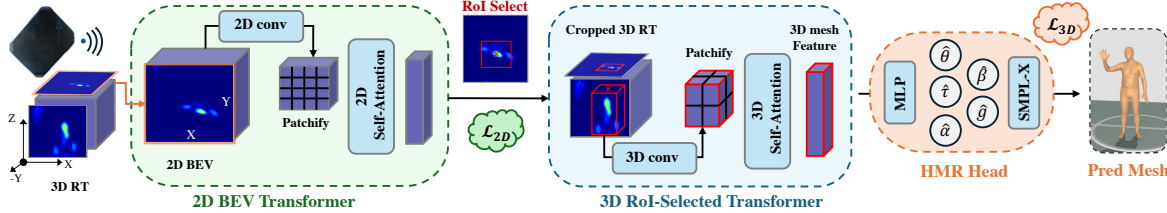


Figure 4. Overview of the proposed RT-Mesh baseline. Given a 3D radar tensor (RT), RT-Mesh first reshapes it into a 2D BEV representation. A lightweight 2D BEV Transformer, combining 2D convolution and self-attention, performs efficient 2D human localization (\hat{x}, \hat{y}) under the supervision of \mathcal{L}_{2D} . A local 3D RoI is cropped from the full RT volume based on (\hat{x}, \hat{y}) , which is then processed by 3D convolution and 3D Transformer to extract fine-grained 3D mesh features. Finally, an HMR head regresses SMPL-X parameters for 3D mesh.

assessing unseen-action generalization.

Metrics. We evaluate the mesh reconstruction performance using four classic metrics, all computed in the *world* frame without root/Procrustes alignment and reported in millimeters/degrees. *Mean Vertex Error (MVE)* is the average Euclidean distance between predicted and ground-truth SMPL-X vertices over all 10,475 vertices. *Mean Joint Error (MJE/MPJPE)* is the mean Euclidean distance between corresponding 3D joints using the 22-joint SMPL-X set. *Mean Rotation Error (MRE)* is the geodesic angular error on $SO(3)$ between predicted and ground-truth joint rotations, averaged across joints; it emphasizes pose and is invariant to global translation. *Translation Error (TE)* is the Euclidean distance between predicted and ground-truth global root translations.

4.2. RT-Mesh: A Baseline for RT-based HMR

Problem Formulation. Following prior works [4, 5, 44], we allow a short temporal context of radar frames. We stack $T = 4$ consecutive RTs, forming a 4D tensor $X_{RT} \in \mathbb{R}^{T \times X \times Y \times Z}$, where $(X, Y, Z) = (121, 111, 31)$ in our dataset. Given X_{RT} , our goal is to regress the SMPL-X parameters $(\alpha, \beta, \tau, \theta)$: root orientation (axis-angle) $\alpha \in \mathbb{R}^3$, body shape $\beta \in \mathbb{R}^{10}$, global translation $\tau \in \mathbb{R}^3$, and body pose $\theta \in \mathbb{R}^{22 \times 3}$. We also regress gender probability $g \in [0, 1]$ to select the appropriate male/female SMPL-X template. Supervision for $(\alpha, \beta, \tau, \theta, g)$ comes from our MoCap-derived mesh annotations (Sec. 3.6).

Model Architecture. We propose **RT-Mesh**, the first HMR method that operates directly on RTs. Compared with RPC, RT retains richer human return signals but at much higher volume, making full-volume 3D/4D convolutions computationally prohibitive. To improve the model efficiency with losing key context information, RT-Mesh is specifically designed as a two-stage structure (c.f. Fig. 4): it first localizes the human foreground RoI amid clutter using a collapsed 2D BEV tensor, then operates on a local 3D RT crop to regress the final SMPL-X mesh parameters. Detailed architecture and training loss designs are provided in the supplementary.

4.3. Competing Methods

RGB(D) Modality. For the RGB setting, we adopt the SOTA TokenHMR method [13] and follow its practices: persons are first detected using Detectron2 [41] and cropped for local mesh recovery. To obtain the best performance, we initialize the model with its large-scale pretrained weights and fine-tune it on our dataset. For the depth setting, we back-project depth pixels to 3D point clouds and apply the point cloud-based HMR method P4Transformer [14].

mmWave Modality. To comprehensively benchmark radar-based HMR, we include SOTA methods from existing mmWave HPE and HMR datasets for both RPC and RT modalities. For RPC-based methods, we select two representative HMR approaches: LSTM-based mmMesh [43] and transformer-based P4Transformer [14] applied in the mmBody [7] dataset. Since no existing HMR method is designed for RT, we adopt SOTA models from the latest RT-based HPE datasets: MMVR [33] and RT-Pose [20]. Specifically, RT-Pose [20] adapts HR-Net to radar, using a high-resolution 3D convolutional network as a backbone. RETR [45] from MMVR extracts features from two complementary views—X-Y BEV and X-Z side view—and fuses them using a transformer-based architecture. We preserve the original RT feature extractors, replace their HPE heads with HMR heads, and retrain the models on our dataset.

5. Results and Discussion

5.1. Radar-based HMR Benchmark

Table 2 compares radar-only HMR methods across two radar modalities, RPC and RT. Under the random split (S1), both modalities performs strongly: P4Trans. (RPC) [7] and RT-Mesh (RT) reach ~ 70 mm MVE on In-Place actions and ~ 90 mm overall, exceeding reported results on prior radar-based HMR/HPE datasets. This underscores the quality of our dataset and shows that high-resolution mmWave radar alone can support accurate HMR in privacy-sensitive or vision-impaired scenarios. Our dataset poses additional challenges for another two protocols and split settings, and resulted in performance drop. P2 (Sit-In-Place) suffers

Table 2. Performance of SOTA radar-based HMR using RPC and RT modalities. The mean vertex error (MVE) (mm) is recorded for all protocols and splits, lower the better. We also include the single-sample Latency (Lat.) and GFLOPs for comparing model efficiency.

Modality	Methods	Efficiency		P1 (In-Place)			P2 (Sit-In-Place)			P3 (Non-In-Place)			ALL		
		Lat. (ms)	GFLOPs	S1	S2	S3	S1	S2	S3	S1	S2	S3	S1	S2	S3
RPC	mm-Mesh [44]	3.53	2.87	105.9	149.4	146.0	183.3	202.8	194.5	201.4	226.8	223.3	132.7	170.1	173.8
	P4Trans. [7]	7.17	11.76	72.7	129.3	132.3	115.2	142.8	132.0	139.7	180.2	184.4	90.4	140.8	147.8
RT	RT-Pose [20]	39.58	50.67	80.0	135.9	133.7	130.2	152.4	139.5	158.5	188.4	196.0	100.7	148.1	152.8
	RETR [45]	17.87	3.01	73.2	159.4	143.0	133.6	169.4	153.6	162.6	206.1	207.0	97.1	169.7	163.1
	RT-Mesh (ours)	2.74	2.60	72.4	123.6	128.5	118.1	138.5	126.5	142.0	173.6	178.2	90.9	135.1	143.1

from frequent self-occlusion and chair-induced multipath noise, while P3 (Non-In-Place) require jointly tracking and pose/mesh estimation under rapid, dynamic motion. S2 (Cross-subject) and S3 (Cross-action) settings also remain challenging, highlighting the need for better generalizability.

Comparing two radar representations, RT and RPC perform similarly on S1, but RT outperforms RPC on S2 and S3, indicating stronger generalizability. RT preserves denser, more continuous spatial evidence, whereas RPC is sparse and susceptible to missed detections of body parts (c.f. Fig. 6). Especially for novel subjects and actions, these gaps can induce overfitting and yield twisted meshes. Moreover, our proposed RT-Mesh attains markedly higher efficiency than existing RPC- and RT-based methods, particularly those that process full-volume RT. It achieves 2.74 ms latency and 2.6 GFLOPs, making it deployable on edge devices. As a simple and efficient baseline, RT-Mesh is designed to encourage exploration into RT-based HMR, which remains an underexplored direction. We believe future work can build on this foundation to develop models with higher spatial precision, temporal consistency, and integration of human priors.

5.2. In Depth Analysis of Dataset Scale

Fig. 5 presents an in-depth analysis of how the training dataset size influences the performance of radar-based HMR.

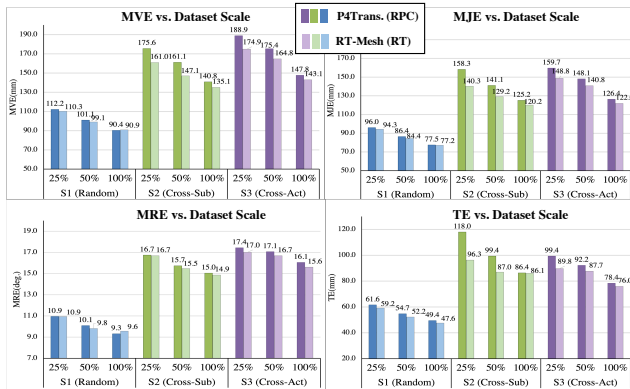


Figure 5. Impact of the training data size to radar-based HMR. Larger dataset consistently improves performance on S2 (cross-subject) and S3 (cross-action) across all evaluation metrics.

We evaluate models trained with 25%, 50%, and 100% of our training data under different split settings, where 25% approximates the size of existing radar HMR datasets such as mmBody [7]. For cross-subject (S2), this corresponds to using 4, 8, and 16 training subjects; for cross-action (S3), we use 10, 20, and 40 training action classes, respectively.

We find that the scaling law [23] holds for mmWave-based HMR: enlarging the training set consistently improves performance across splits and metrics, particularly for S2 and S3. For instance, RT-Mesh improves from 161.0mm to 135.1mm MVE on S2, and from 174.9mm to 143.1mm on S3. A richer dataset provides essential diversity for learning robust mappings between human motion and radar reflections, which helps mitigate the common challenges of multi-path interference and body-part miss-detection inherent to RF sensing. These results demonstrate the importance of large-scale training data in advancing mmWave-based human sensing and modelling, potentially enabling hard use cases (e.g., HMR for sports) and narrowing the gap to RGB-D systems.

5.3. Comparison to RGB(D)-based Methods

Table 3 (Single) compares the best RPC- and RT-based model against RGB(D)-based methods (c.f. Sec. 4.3). With higher-resolution radar, radar-only models achieve comparable performance to RGB-D. Under S1 and S2, radar surpasses RGB and approaches depth. Notably, the translation error (TE) of radar matches depth and clearly outperforms RGB, which lacks explicit range information. We attribute this to radar's higher sensitivity to moving foreground and suppression of static background, yielding more reliable root tracking in fast, non-in-place motions. Under S2 and S3, all modalities degrades largely, indicating that generalization to unseen subjects/actions remains difficult, even for camera-based HMR models that benefit from large-scale pretraining. We expect M4Human to serve as a strong benchmark for advancing generalizable HMR across all modalities.

5.4. Multimodal Fusion

Table 3 (Fusion) benchmarks multi-modal fusion for HMR. For this experiment, we apply intermediate feature fusion, where features from each modality are concatenated before the HMR prediction head. On S1 and S3, RPC+RT remarkably outperforms either RPC or RT alone. This result

Table 3. Performance of different single modalities and multi-modality fusion under protocol ALL and 3 different splits. All four metrics are reported to reflect advantages of different modality, lower the better.

Modality	Protocol	S1 (Random)				S2 (Cross-Sub)				S3 (Cross-Act)				
		MVE	MJE	MRE	TE	MVE	MJE	MRE	TE	MVE	MJE	MRE	TE	
Single	ALL	RGB	97.5	87.0	7.4	54.4	149.7	128.4	9.3	99.2	116.7	110.6	10.0	82.7
		Depth	82.7	72.1	9.1	45.6	127.1	115.5	14.4	89.1	123.2	106.9	14.4	61.2
		RPC	89.5	76.6	9.2	48.6	140.8	125.2	15.0	86.4	147.8	126.4	16.1	78.4
		RT	90.9	77.2	9.6	47.6	135.1	120.2	14.9	86.1	143.1	122.0	15.6	76.0
Fusion	ALL	RPC + RT	84.3	71.7	8.9	43.8	135.2	119.3	15.0	85.7	140.8	120.9	15.5	73.4
		RGB + RT	80.1	71.4	8.9	51.6	112.5	103.2	11.6	80.5	108.7	98.4	11.5	75.7
		Depth + RT	77.5	66.3	8.4	36.0	115.9	102.6	14.0	72.2	120.0	102.4	14.6	56.6

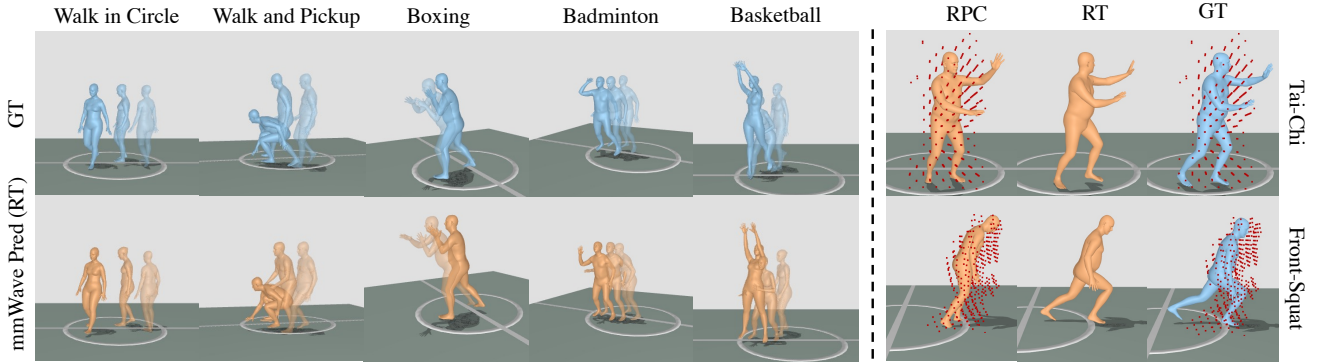


Figure 6. Visualization of (left) RT-based HMR under challenging (P3) non-in-place actions, and (right) comparison between RPC and RT predicted meshes. The proposed RT-Mesh can simultaneously track and reconstruct 3D human meshes during complex sports motions. In contrast, RPC-based prediction may fail when points are missing for certain body parts.

Table 4. Benchmark on downstream skeleton-based human action recognition (HAR) out of 50 actions. We show the Top-1 and Top-5 accuracy (%) using GT skeletons on S1, radar tensor (RT) predicted skeletons on S1 and S2.

Methods	GT (S1)		RT (S1)		RT (S2)	
	Top-1	Top-5	Top-1	Top-5	Top-1	Top-5
CNN [12]	53.55	80.76	37.73	51.37	41.26	51.14
AGCN [36]	65.70	94.24	64.82	90.55	59.91	83.97
BlockGCN [52]	75.67	95.22	61.06	87.75	27.85	51.01

highlights the complementary value of RT and underscores the significance of M4Human as the first dataset supporting RT-based HMR. We argue that learning jointly from two radar representations is mutually reinforcing: RT preserves dense spatial context while RPC emphasizes salient targets with pronounced motion. Moreover, fusing RT with RGB and depth images also yield significant gains, especially in TE for root-trajectory tracking. This demonstrates that radar can be a strong complementary modality to many camera-based systems for real-world applications.

5.5. Downstream HAR Benchmark

Table 4 evaluates skeleton-based HAR with two inputs: (i) MoCap-de skeletons GT and (ii) RT-estimated skeletons extracted from meshes predicted by RT-Mesh. Under S1 (random split), BlockGCN [52] attains $\sim 75\%$ Top-1 accu-

racy using MoCap skeletons, highlighting that our dataset is challenging due to dynamic, non-in-place actions. Moreover, RT-estimated skeletons already exhibit considerable accuracy, reaching 64.82% (Top-1), indicating that the proposed RT-Mesh can effectively support downstream HAR. Cross-subject generalization is still challenging for radar-based HAR, given additional performance drops in S2.

6. Conclusion

We present M4Human, a large-scale multimodal benchmark for mmWave radar-based human mesh reconstruction. The dataset comprises 661K synchronized frames spanning 50 actions and 20 subjects, captured with high-resolution mmWave radar, RGB, and depth modalities, and annotated with marker-based 3D meshes. M4Human provides both raw radar tensors (RT) and radar point clouds (RPC) to enabling research across different RF representation levels. We also propose RT-Mesh, a simple but effective baseline—the first method to perform HMR directly from raw RTs. Extensive experiments establish single- and multi-modal benchmarks across radar and RGB-D modalities, revealing the potential of mmWave radar for fine-grained, privacy-preserving human sensing. We expect M4Human to serve as a foundation for advancing RF-based 3D human modeling and its applications in Physical AI systems.

References

- [1] Vayyar imaging - home - vayyar, 2023. [4](#)
- [2] Mohammad Arif Ul Alam, Md Mahmudur Rahman, and Jared Q Widberg. Palmar: Towards adaptive multi-inhabitant activity recognition in point-cloud technology. In *IEEE INFOCOM 2021-IEEE conference on computer communications*, pages 1–10. IEEE, 2021. [3](#)
- [3] Sizhe An and Umit Y Ogras. Mars: mmwave-based assistive rehabilitation system for smart healthcare. *ACM Transactions on Embedded Computing Systems (TECS)*, 20(5s):1–22, 2021. [2, 3](#)
- [4] Sizhe An and Umit Y Ogras. Fast and scalable human pose estimation using mmwave point cloud. In *Proceedings of the 59th ACM/IEEE Design Automation Conference*, pages 889–894, 2022. [6](#)
- [5] Sizhe An, Yin Li, and Umit Ogras. mri: Multi-modal 3d human pose estimation dataset using mmwave, rgb-d, and inertial sensors. *Advances in neural information processing systems*, 35:27414–27426, 2022. [2, 3, 6](#)
- [6] Andrea Avogaro, Federico Cunico, Bodo Rosenhahn, and Francesco Setti. Markerless human pose estimation for biomedical applications: a survey. *Frontiers in Computer Science*, 5:1153160, 2023. [1](#)
- [7] Anjun Chen, Xiangyu Wang, Shaohao Zhu, Yanxu Li, Jiming Chen, and Qi Ye. mmbbody benchmark: 3d body reconstruction dataset and analysis for millimeter wave radar. In *Proceedings of the 30th ACM International Conference on Multimedia*, pages 3501–3510, 2022. [2, 3, 4, 6, 7](#)
- [8] Haoming Chen, Runyang Feng, Sifan Wu, Hao Xu, Fengcheng Zhou, and Zhenguang Liu. 2d human pose estimation: A survey. *Multimedia Systems*, 29(5):3115–3138, 2023. [2](#)
- [9] Han Cui and Naim Dahnoun. High precision human detection and tracking using millimeter-wave radars. *IEEE Aerospace and Electronic Systems Magazine*, 36(1):22–32, 2021. [3](#)
- [10] Fangqiang Ding, Zhen Luo, Peijun Zhao, and Chris Xiaoxuan Lu. milliflow: Scene flow estimation on mmwave radar point cloud for human motion sensing. In *European Conference on Computer Vision*, pages 202–221. Springer, 2024. [3](#)
- [11] Fangqiang Ding, Yunzhou Zhu, Xiangyu Wen, Gaowen Liu, and Chris Xiaoxuan Lu. Thermohands: A benchmark for 3d hand pose estimation from egocentric thermal images. In *Proceedings of the 23rd ACM Conference on Embedded Networked Sensor Systems*, pages 533–546, 2025. [2](#)
- [12] Yong Du, Yun Fu, and Liang Wang. Skeleton based action recognition with convolutional neural network. In *2015 3rd IAPR Asian conference on pattern recognition (ACPR)*, pages 579–583. IEEE, 2015. [8](#)
- [13] Sai Kumar Dwivedi, Yu Sun, Priyanka Patel, Yao Feng, and Michael J Black. Tokenhmr: Advancing human mesh recovery with a tokenized pose representation. In *Proceedings of the IEEE/CVF conference on computer vision and pattern recognition*, pages 1323–1333, 2024. [2, 6](#)
- [14] Hehe Fan, Yi Yang, and Mohan Kankanhalli. Point 4d transformer networks for spatio-temporal modeling in point cloud videos. In *Proceedings of the IEEE/CVF conference on computer vision and pattern recognition*, pages 14204–14213, 2021. [6](#)
- [15] Junqiao Fan, Jianfei Yang, Yuecong Xu, and Lihua Xie. Diffusion model is a good pose estimator from 3d rf-vision. In *European Conference on Computer Vision*, pages 1–18. Springer, 2024. [3](#)
- [16] Martin A Fischler and Robert C Bolles. Random sample consensus: a paradigm for model fitting with applications to image analysis and automated cartography. *Communications of the ACM*, 24(6):381–395, 1981. [4](#)
- [17] Daniel R Fuhrmann, Edward J Kelly, and Ramon Nitzberg. A cfar adaptive matched filter detector. *IEEE Trans. Aerosp. Electron. Syst.*, 28(1):208–216, 1992. [2, 4](#)
- [18] Nima Ghorbani and Michael J Black. Soma: Solving optical marker-based mocap automatically. In *Proceedings of the IEEE/CVF International Conference on Computer Vision*, pages 11117–11126, 2021. [5](#)
- [19] Tianbo Gu, Zheng Fang, Zhicheng Yang, Pengfei Hu, and Prasant Mohapatra. Mmsense: Multi-person detection and identification via mmwave sensing. In *Proceedings of the 3rd ACM Workshop on Millimeter-wave Networks and Sensing Systems*, pages 45–50, 2019. [3](#)
- [20] Yuan-Hao Ho, Jen-Hao Cheng, Sheng Yao Kuan, Zhongyu Jiang, Wenhao Chai, Hsiang-Wei Huang, Chih-Lung Lin, and Jenq-Neng Hwang. Rt-pose: A 4d radar tensor-based 3d human pose estimation and localization benchmark. In *European Conference on Computer Vision*, pages 107–125. Springer, 2024. [2, 3, 6, 7](#)
- [21] Intel RealSense. Depth Camera D455. <https://www.intelrealsense.com/depth-camera-d455/>, 2023. Accessed: 2024-02-27. [3](#)
- [22] Catalin Ionescu, Dragos Papava, Vlad Olaru, and Cristian Sminchisescu. Human3. 6m: Large scale datasets and predictive methods for 3d human sensing in natural environments. *IEEE transactions on pattern analysis and machine intelligence*, 36(7):1325–1339, 2013. [2, 3](#)
- [23] Jared Kaplan, Sam McCandlish, Tom Henighan, Tom B Brown, Benjamin Chess, Rewon Child, Scott Gray, Alec Radford, Jeffrey Wu, and Dario Amodei. Scaling laws for neural language models. *arXiv preprint arXiv:2001.08361*, 2020. [7](#)
- [24] Łukasz Kidziński, Bryan Yang, Jennifer L Hicks, Apoorva Rajagopal, Scott L Delp, and Michael H Schwartz. Deep neural networks enable quantitative movement analysis using single-camera videos. *Nature communications*, 11(1):4054, 2020. [5](#)
- [25] Muhammed Kocabas, Nikos Athanasiou, and Michael J Black. Vibe: Video inference for human body pose and shape estimation. In *Proceedings of the IEEE/CVF conference on computer vision and pattern recognition*, pages 5253–5263, 2020. [2](#)
- [26] Shih-Po Lee, Niraj Prakash Kini, Wen-Hsiao Peng, Ching-Wen Ma, and Jenq-Neng Hwang. Hupr: A benchmark for human pose estimation using millimeter wave radar. In *Proceedings of the IEEE/CVF Winter Conference on Applications of Computer Vision*, pages 5715–5724, 2023. [3](#)

[27] Yadong Li, Dongheng Zhang, Jinbo Chen, Jinwei Wan, Dong Zhang, Yang Hu, Qibin Sun, and Yan Chen. Towards domain-independent and real-time gesture recognition using mmwave signal. *IEEE Transactions on Mobile Computing*, 22(12):7355–7369, 2022. 3

[28] Haipeng Liu, Yuheng Wang, Anfu Zhou, Hanyue He, Wei Wang, Kunpeng Wang, Peilin Pan, Yixuan Lu, Liang Liu, and Huadong Ma. Real-time arm gesture recognition in smart home scenarios via millimeter wave sensing. *Proceedings of the ACM on interactive, mobile, wearable and ubiquitous technologies*, 4(4):1–28, 2020. 3

[29] Yang Liu, Changzhen Qiu, and Zhiyong Zhang. Deep learning for 3d human pose estimation and mesh recovery: A survey. *Neurocomputing*, 596:128049, 2024. 2

[30] Dushyant Mehta, Helge Rhodin, Dan Casas, Pascal Fua, Oleksandr Sotnychenko, Weipeng Xu, and Christian Theobalt. Monocular 3d human pose estimation in the wild using improved cnn supervision. In *2017 international conference on 3D vision (3DV)*, pages 506–516. IEEE, 2017. 3

[31] Catherine Morgan, Emma L Tonkin, Alessandro Masullo, Ferdinand Jovan, Arindam Sikdar, Pushpajit Khaire, Majid Mirmehdi, Ryan McConville, Gregory JL Tourte, Alan Whone, et al. A multimodal dataset of real world mobility activities in parkinson’s disease. *Scientific data*, 10(1):918, 2023. 2

[32] Georgios Pavlakos, Vasileios Choutas, Nima Ghorbani, Timo Bolkart, Ahmed AA Osman, Dimitrios Tzionas, and Michael J Black. Expressive body capture: 3d hands, face, and body from a single image. In *Proceedings of the IEEE/CVF conference on computer vision and pattern recognition*, pages 10975–10985, 2019. 5

[33] M Mahbubur Rahman, Ryoma Yataka, Sorachi Kato, Pu Wang, Peizhao Li, Adriano Cardace, and Petros Boufounos. Mmvr: Millimeter-wave multi-view radar dataset and benchmark for indoor perception. In *European Conference on Computer Vision*, pages 306–322. Springer, 2024. 2, 3, 6

[34] Sandeep Rao. Introduction to mmwave sensing: Fmcw radars. *Texas Instruments (TI) mmWave Training Series*, pages 1–11, 2017. 2, 4

[35] Arindam Sengupta, Feng Jin, Renyuan Zhang, and Siyang Cao. mm-pose: Real-time human skeletal posture estimation using mmwave radars and cnns. *IEEE sensors journal*, 20(17):10032–10044, 2020. 3

[36] Lei Shi, Yifan Zhang, Jian Cheng, and Hanqing Lu. Two-stream adaptive graph convolutional networks for skeleton-based action recognition. In *Proceedings of the IEEE/CVF conference on computer vision and pattern recognition*, pages 12026–12035, 2019. 8

[37] Akash Deep Singh, Sandeep Singh Sandha, Luis Garcia, and Mani Srivastava. Radhar: Human activity recognition from point clouds generated through a millimeter-wave radar. In *Proceedings of the 3rd ACM Workshop on Millimeter-wave Networks and Sensing Systems*, pages 51–56, 2019. 3

[38] Jan Stenum, Kendra M Cherry-Allen, Connor O Pyles, Rachel D Reetzke, Michael F Vignos, and Ryan T Roemich. Applications of pose estimation in human health and performance across the lifespan. *Sensors*, 21(21):7315, 2021. 1

[39] Yating Tian, Hongwen Zhang, Yebin Liu, and Limin Wang. Recovering 3d human mesh from monocular images: A survey. *IEEE transactions on pattern analysis and machine intelligence*, 45(12):15406–15425, 2023. 2

[40] Timo Von Marcard, Roberto Henschel, Michael J Black, Bodo Rosenhahn, and Gerard Pons-Moll. Recovering accurate 3d human pose in the wild using imus and a moving camera. In *Proceedings of the European conference on computer vision (ECCV)*, pages 601–617, 2018. 2, 3

[41] Yuxin Wu, Alexander Kirillov, Francisco Massa, Wan-Yen Lo, and Ross Girshick. Detectron2. <https://github.com/facebookresearch/detectron2>, 2019. 6

[42] Zhi Wu, Dongheng Zhang, Chunyang Xie, Cong Yu, Jinbo Chen, Yang Hu, and Yan Chen. Rfmask: A simple baseline for human silhouette segmentation with radio signals. *IEEE Transactions on Multimedia*, 25:4730–4741, 2022. 3

[43] Hongfei Xue, Yan Ju, Chenglin Miao, Yijiang Wang, Shiyang Wang, Aidong Zhang, and Lu Su. mmmesh: Towards 3d real-time dynamic human mesh construction using millimeter-wave. In *Proceedings of the 19th Annual International Conference on Mobile Systems, Applications, and Services*, pages 269–282, 2021. 2, 3, 6

[44] Jianfei Yang, He Huang, Yunjiao Zhou, Xinyan Chen, Yuecong Xu, Shanghai Yuan, Han Zou, Chris Xiao-xuan Lu, and Lihua Xie. Mm-fi: Multi-modal non-intrusive 4d human dataset for versatile wireless sensing. *arXiv preprint arXiv:2305.10345*, 2023. 2, 3, 6, 7

[45] Ryoma Yataka, Adriano Cardace, Perry Wang, Petros Boufounos, and Ryuhei Takahashi. Retr: Multi-view radar detection transformer for indoor perception. *Advances in Neural Information Processing Systems*, 37:19839–19869, 2024. 3, 6, 7

[46] Jia Zhang, Rui Xi, Yuan He, Yimiao Sun, Xiuzhen Guo, Weiguo Wang, Xin Na, Yunhao Liu, Zhenguo Shi, and Tao Gu. A survey of mmwave-based human sensing: Technology, platforms and applications. *IEEE Communications Surveys & Tutorials*, 2023. 2

[47] Jiarui Zhang, Songnan Lin, Hao Cheng, Weixian Liu, and Bihan Wen. Learning-based human detection via radar for dynamic and cluttered indoor environments. In *2024 IEEE International Symposium on Circuits and Systems (ISCAS)*, pages 1–5. IEEE, 2024. 3

[48] Mingmin Zhao, Yonglong Tian, Hang Zhao, Mohammad Abu Alsheikh, Tianhong Li, Rumen Hristov, Zachary Kabelac, Dina Katabi, and Antonio Torralba. Rf-based 3d skeletons. In *Proceedings of the 2018 Conference of the ACM Special Interest Group on Data Communication*, pages 267–281, 2018. 2, 3

[49] Peijun Zhao and Hermano Igo Krebs. Enabling home rehabilitation with smartphone-powered upper limb training. In *2024 10th IEEE RAS/EMBS International Conference for Biomedical Robotics and Biomechatronics (BioRob)*, pages 438–443. IEEE, 2024. 5

[50] Peijun Zhao, Chris Xiao-xuan Lu, Jianan Wang, Changhao Chen, Wei Wang, Niki Trigoni, and Andrew Markham. mid: Tracking and identifying people with millimeter wave radar. In *2019 15th International Conference on Distributed Com-*

puting in Sensor Systems (DCOSS), pages 33–40. IEEE, 2019.

3

- [51] Ce Zheng, Wenhan Wu, Chen Chen, Taojiannan Yang, Si-jie Zhu, Ju Shen, Nasser Kehtarnavaz, and Mubarak Shah. Deep learning-based human pose estimation: A survey. *ACM computing surveys*, 56(1):1–37, 2023. 1
- [52] Yuxuan Zhou, Xudong Yan, Zhi-Qi Cheng, Yan Yan, Qi Dai, and Xian-Sheng Hua. Blockgen: Redefine topology awareness for skeleton-based action recognition. In *Proceedings of the IEEE/CVF Conference on Computer Vision and Pattern Recognition*, pages 2049–2058, 2024. 8